Fakultät für Physik
Technische Universität München

Walter Schottky Institute
Technical University of Munich

SEMICONDUCTOR PHOTOELECTROCHEMISTRY

Advanced Lab Course

Viktoria Kunzelmann
Viktoria.Kunzelmann@wsi.tum.de

Prof. Dr. Ian Sharp
Sharp@wsi.tum.de
Chair for Experimental Semiconductor Physics
Walter Schottky Institute
Technical University of Munich
Am Coulombwall 4, 85748 Garching

Contents

1 Introduction and learning outcomes

Traditional electrochemistry is based on electrically conducting electrodes that are placed in contact with an ionic conductor, which is often a liquid electrolyte. Under an applied electrical bias, such systems are capable of driving electrochemical redox reactions at electrode/electrolyte interfaces. To complete the conducting circuit, two electrodes are required: an anode that is responsible for the oxidation half-reaction and a cathode that is responsible for the reduction half-reaction. These configurations form the basis for several important technologies, including batteries, electrolyzers, and fuel cells. However, interesting questions arise if we consider what happens if one or both of these conducting electrodes is replaced by a semiconductor – the type of material that forms the basis for modern microprocessors, light emitting diodes, and solar cells (to name just a few key technologies). Such materials are characterized by an electronic bandgap, broadly tunable electrical conductivity, and the ability to develop or maintain internal electric fields. In addition, they can be photoactive, meaning that there is an appreciable change of the charge carrier concentration within the material when it is excited by photons possessing energies above the bandgap energy. As a consequence, we would expect electrochemical characteristics for these electrodes to be a strong function of their illumination condition; that is, these semiconductor electrodes may be considered to be *photoelectrodes*. Since the chemical transformations that occur at the surfaces of these photoelectrodes are a strong function of the chemical composition of the electrolyte and the electrical bias (i.e. the electrochemical potential), as well as illumination, the study of these systems is known as *semiconductor photoelectrochemistry*.

Although it was not identified as such at the time, semiconductor photoelectrochemistry dates back to some of the earliest experiments on the nature of electricity. In his pioneering experiment of 1839, the French physicist Edmond Becquerel observed that a voltage develops when a silver chloride electrode, immersed in an acidic electrolyte and connected to a platinum metal counter electrode, is illuminated. The discovery of this phenomenon, now termed the photovoltaic effect, laid the foundation for the development of modern solar cells. More than 120 years later, in 1972, Fujishima and Honda found that a similar process at the interface between semiconducting TiO_2 and an alkaline electrolyte can be used to split water into its elemental constituents, oxygen and hydrogen. This advance launched the modern era of semiconductor photoelectrochemistry research, which today focuses on using illuminated semiconductor/liquid interfaces to generate chemical fuels from sunlight in a process that is often referred to as artificial photosynthesis.

In their simplest configurations, artificial photosystems are designed to sustainably produce hydrogen from sunlight via the splitting of water. In more advanced systems, carbon dioxide can be converted to various carbon-based chemicals, including hydrocarbons and alcohols. Regardless of the chemical product, the key function is to store energy from the sun in the form of chemical bonds, which possess very high energy density. The advantage of doing this is highlighted in Figure 1, which compares the energy densities of different storage media.

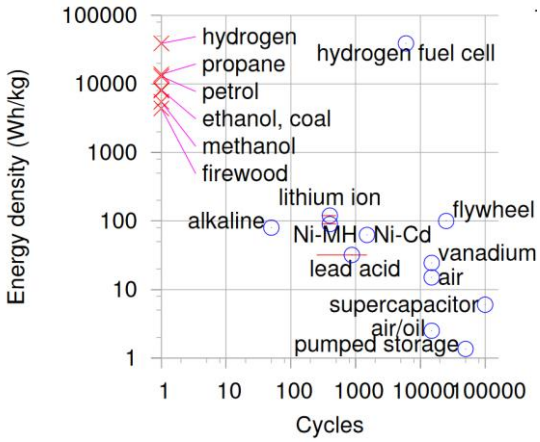

Figure 1: Energy densities (on a logarithmic scale) of energy storage systems such as fuels and typical battery types versus lifetime (number of cycles) [1].

As can be seen here, chemical fuels possess dramatically higher energy densities than batteries. Thus, artificial photosynthesis based on semiconductor photoelectrochemistry addresses two major limitations of traditional solar cells. First, it provides high energy density fuels that can be used for long range transportation where batteries are insufficient, such as for aircraft, ships, and trucks. Second, it provides a path to large scale storage of solar energy to overcome the problem of intermittent daily and seasonal power generation from the Sun.

Despite the alluring prospect of artificial photosystems for storing the energy of sunlight in chemical bonds of fuels, there remain considerable challenges to practical implementation. In particular, devices must be created that are simultaneously efficient, stable, and scalable. Although materials and combinations of materials exist that can fulfill different subsets of these requirements, no system has yet been found to satisfy all three. Thus, modern research in physics, chemistry, materials, and engineering seeks to address this central challenge. Here, it is important to recognize that semiconductors form the heart of artificial photosynthesis systems. These materials are used to absorb solar energy, separate photogenerated charge carriers in specific directions, and drive electrochemical reactions using these separated charge carriers. The first of these two processes are similar to those occurring in traditional solid state solar cells. However, the third process is unique to photoelectrochemical energy conversion and leads to a coupling of electrical and chemical processes at the solid/liquid interface.

In this laboratory module, you will learn the fundamental characteristics of semiconductor/liquid interfaces, including both interfacial energetic alignment and the competitive kinetics of photocarrier recombination and chemical reaction that are unique to such systems. You will gain practical experience with assembling and operating photoelectrochemical cells, which include the electrodes (working, counter, and reference), potentiostat, and solar simulator. Using a state-of-the-art transition metal oxide semiconductor, bismuth vanadate ($BiVO_4$), you will determine and understand how photoelectrochemical current varies as a function of electrochemical bias and illumination. Armed with this information, you will be able to describe the physical mechanisms that limit its efficiency, as well as the stability of the system. This knowledge will allow you to understand some of the key aspects of photoelectrochemical energy conversion and provide a foundation for critically analyzing modern research on the subject.

This manual below provides a brief introduction to basics of semiconductor/electrolyte interfaces, followed by a description and procedure for experiments.

2 Theoretical background

Before addressing the complex energetic situation in a semiconductor during photoelectrochemical energy conversion, the fundamental energy landscape at a semiconductor surface in the dark and under illumination is described. Basic knowledge of semiconductors and Fermi statistics is assumed, though a brief summary is provided as a refresher.

2.1 Electronic levels of semiconductor surfaces in the dark and under illumination

An ideal crystal is characterized by an infinite periodic repetition of its constituent atoms, which ultimately gives rise to the electronic band structure of the material. The details of this band structure, as well as the occupation of the energetic bands by electrons, defines the electrical and optical properties of the ideal material. For the case of a semiconductor, the bandgap, E_g, defines the energetic separation between the occupied states of the valence band and the unoccupied states of the conduction band. For a pure semiconductor in the absence of defects, the Fermi level, E_F, lies near the middle of the bandgap. For such a case, the semiconductor is said to be intrinsic. However, the presence of defects and impurities can introduce electronic states within the bandgap. At finite temperature, so-called donor states provide additional electrons to the conduction band and acceptor states provide additional holes to the valence band. For a semiconductor with an excess of electrons, the Fermi level moves towards the conduction band edge, and the material is called n-type. Likewise, for a semiconductor with an excess of holes, the Fermi level moves towards the valence band edge, and the material is called p-type.

The considerations above define the electronic properties of the bulk of a crystalline semiconductor. However, at surfaces the periodic atomic symmetry of the crystal is abruptly terminated, which leads to the presence of under- and non-ideally coordinated atoms. At unpassivated surfaces, unpaired electrons in dangling bonds of surface atoms interact with each other and form new electronic states. When these states lie within the bandgap of the material, which is usually the case, they are electronically active and are referred to as surface states. Since these surface states have an energy distribution within the semiconductor band gap, the position of the Fermi level with respect to the valence and conduction band edges is different at the surface than in the bulk of the material. For nearly all semiconductor devices, charge carriers must be either injected or extracted across interfaces and, thus, surface states can play a decisive role in optoelectronic processes. As we will see below, for the case of semiconductor photoelectrodes this is especially true, since the interfacial electronic properties are not only responsible for charge extraction, but also charge separation.

Figure 2 illustrates the energy bands of an n- and p-type semiconductor near the surface in disequilibrium and in equilibrium. It is assumed that the surface states are half filled and centered at the middle of the band gap. For an n-type semiconductor, the bulk Fermi level E_F(bulk) lies close to the conduction band (CB), but is energetically above the Fermi level of the surface, E_F(surf). In order to achieve equilibrium, electrons will transfer from the bulk to the surface. As a result, E_F(bulk) will decrease and E_F(surf) increase until they are aligned in equilibrium. The consequence is an upward band bending of the CB and valence band (VB) from bulk towards the surface (Figure 2 (b).) For p-type semiconductors, the bulk Fermi level is located close to the valence band (Figure 2(c)), causing electrons to flow from the surface to the bulk and resulting in a downward band bending towards the surface at equilibrium (Figure 2(d)).

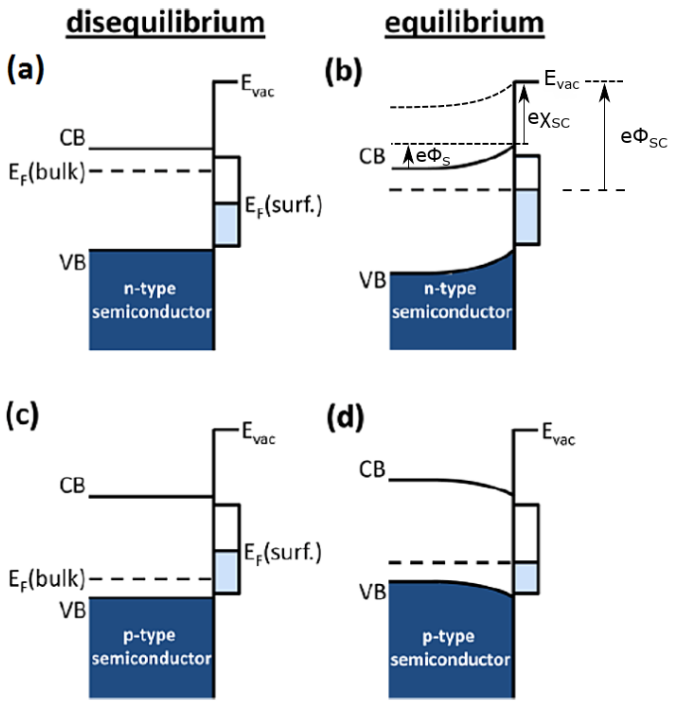

Figure 2: Energy levels near the surface of (a) an n-type semiconductor in disequilibrium and (b) in equilibrium with the surface. In equilibrium, the semiconductor Fermi level E_F (bulk) and the surface Fermi level E_F (surf) align and an upward band bending occurs. (c) and (d) show the inverted situation for a p-type semiconductor where a downward band bending results. Figure adapted from [2].

As illustrated in Figure 2(b) for an n-type semiconductor, the band bending on the surface can be described by its built-in potential, $e\Phi_S$, and the width, W, of the associated space charge region (SCR). The work function of the semiconductor can be expressed by considering the electron affinity of the semiconductor, $e\chi_{SC}$, which defines the energy difference between the CB edge (E_C) and the vacuum level (E_{vac}), as well as the Fermi level E_F, as:

$$e\Phi_{SC} = e\chi_{SC} + e\Phi_S + (E_C - E_F)$$

where e is the elementary charge. The work function, $e\Phi_{SC}$, describes the minimum energy required for an electron to escape the solid and reach the vacuum level E_{vac}. Similar arguments can be used to define the work function of a p-type semiconductor.

Figure 2(b) and Figure 2(d) assume that the system is in equilibrium and that the semiconductor surface is exposed to an inert surrounding (e.g. vacuum). However, the photoelectrodes examined in this laboratory are far from this simple condition. Namely, they are illuminated by photons with energies above the bandgap, they are electrically biased, and they are in contact with a liquid electrolyte with chemical reactions occurring at the solid/liquid interface. Each of these will be described below, but we first continue our discussion by considering the ideal semiconductor surface that is taken out of equilibrium by illumination with photons.

Above-band gap illumination

When the semiconductor is illuminated with photons of energy higher than the band gap energy, electron-hole pairs are created via a band-to-band transition (see Figure 3(a)). In particular, electrons are excited from the valence band to the conduction band, yielding an excess electron in the

conduction band and an excess hole in the valence band. The details of this excitation process (i.e. indirect or direct) depend on the electronic band structure, but will not be discussed further here.

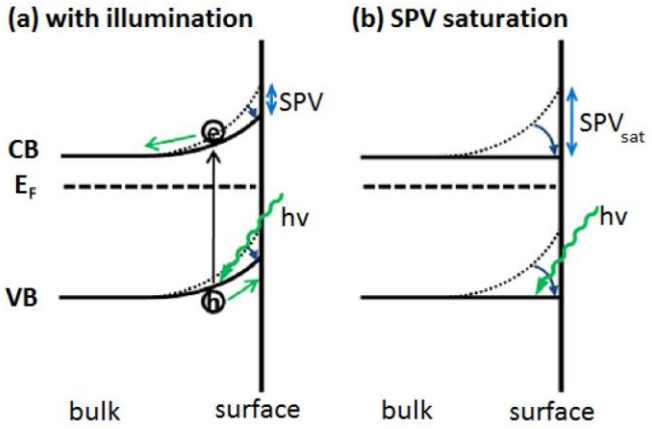

Figure 3: Photoexcitation of an n-type semiconductor by photons of energy higher than the band gap energy. The resulting change in the band bending (surface photovoltage, SPV) is maximized when SPV saturation is reached and the flatband condition prevails. Figure adapted from [2].

The internal electric field within the SCR near the surface, creates an asymmetry within the system that leads to directional charge transport and allows the separation of photogenerated electrons and holes. In particular, for an n-type semiconductor the electric field associated with the band bending causes electrons to drift towards the bulk, whereas holes drift the surface. The corresponding accumulation of holes below the surface has two consequences. First, it can partially shield the negative surface charge, and second, trapping of the holes can lead to a compensation of the negative surface charge. As a result of these two effects, the built-in potential (i.e. the magnitude of band bending) is reduced. This change of the work function due to illumination is called surface photovoltage (SPV). For a sufficiently high photon flux, the band bending can be reduced to zero and the saturation value SPV_{sat} of the surface photovoltage is equal to the initial magnitude of the band bending (Figure 3(b)). The surface photovoltage is an important value for photoelectrodes since it provides an indication for the driving force for charge carrier separation and for the statistical energy of the holes that participate in chemical reactions at the interface. This statistical distribution can be rigorously formulated by considering the so-called quasi-Fermi level of the holes with respect to the quasi-Fermi level of electrons. Although quasi-Fermi levels are not presented in detail here, it should be noted that rigorously, the SPV is given by the quasi-Fermi level splitting that is induced by illumination of the material.

2.2 Electrical contacts to a semiconductor: the metal/semiconductor interface

Electrical contacts form a critical component of nearly all semiconductor-based devices. For the case of semiconductor photoelectrodes, ohmic electrical contacts are used to extract majority carriers from the back surface. Not only is understanding metal/semiconductor junctions necessary for the reliable formation of such contacts, but it also provides a useful foundation for learning about semiconductor/electrolyte contacts that form the rectifying front surface of a semiconductor photoelectrode. In the discussion below, an ideal situation in which the semiconductor is free from surface states, as well as interface dipoles, is assumed, as shown in Figure 4.

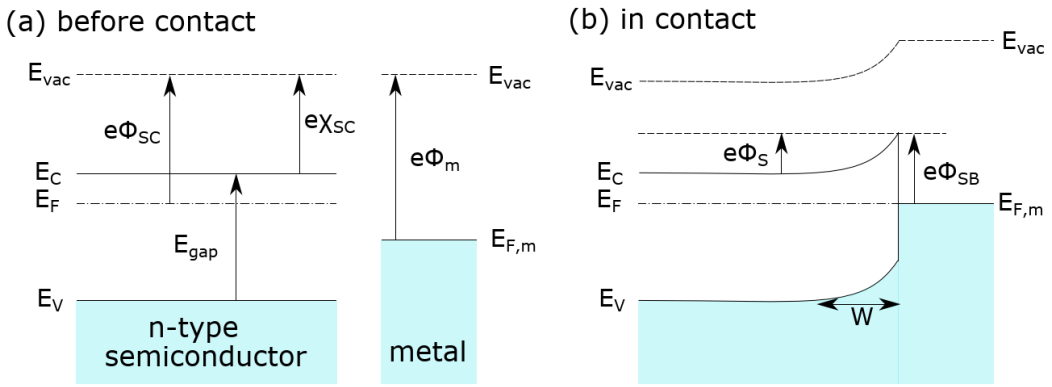

Figure 4: Schematic band structure of a metal-semiconductor junction dominated by bulk properties of an n-type semiconductor. In (a), metal and semiconductor are spatially separated and not in contact and in (b) in contact. Figure inspired by [3].

The metal work function, $e\Phi_m$, is the energy difference between the Fermi level of the metal, $E_{F,m}$, and the vacuum energy, E_{vac}, (see Figure 4(a)) [11]. When a metal and a semiconductor are brought into contact, their Fermi levels will equilibrate (see Figure 4(b)). The following discussion will be for an n-type semiconductor, the p-type case follows in an equivalent way if not stated otherwise. When $E_F > E_{F,m}$, electrons will flow from the semiconductor to the metal, resulting in an electron depletion layer with ionized donor atoms and a SCR of width W. This causes an upward band bending near the semiconductor surface, similar to that described above for the case of defects on a bare semiconductor surface. Due to the short screening length of the high electron density in metals, the extent of the band bending on the metal side is negligible. The potential barrier for majority charge carriers at the metal/semiconductor interface is also called Schottky barrier, named after Walter Schottky who first suggested a theory for rectifying semiconductor contacts in 1938 [4], and is given by the difference of $e\Phi_m$ and $e\chi_{SC}$:

$$e\Phi_{SB,n} = e\Phi_m - e\chi_{SC}$$

For a p-type semiconductor with downward band bending near the interface, $e\phi_{SB,p}$ is defined as:

$$e\Phi_{SB,p} = e\chi_{SC} + E_g - e\Phi_m$$

However, the model described above is simplified and does not consider surface states or metal-induced gap states. In non-ideal systems, the presence of high concentrations of surface or interface states can "pin" the Fermi level near the center of the band gap, independent of the doping type [13]. This can lead to Schottky barrier heights that are only weakly dependent on the metal work function. In such a case, the charging of surface states leads to an interfacial dipole between the metal and semiconductor that allows Fermi level alignment between the metal and semiconductor. While this effect is important in many systems, it will not be discussed further in detail here.

The width, W, of the SCR is dependent on the built-in voltage, Φ_S, and the donor or acceptor concentration $N_{D/A}$ for the corresponding semiconductor doping type, and can be calculated for n- or p-type doping as [14]:

$$W_n = \sqrt{\frac{2\epsilon_r\epsilon_0}{eN_D} \cdot (\Phi_S - U - \frac{k_B T}{e})} \quad \text{(n-type semiconductor)}$$

$$W_p = \sqrt{\frac{2\epsilon_r\epsilon_0}{eN_A} \cdot (-\Phi_S + U + \frac{k_B T}{e})} \quad \text{(p-type semiconductor)}$$

where ε_r and ε_0 are the relative and the vacuum permittivity, repectively, e the elementary charge, k_B the Boltzmann constant, T the temperature, and U the applied external potential. As can be seen in the equation above, the built-in voltage, Φ_S, can be decreased by applying a positive external voltage (with respect to the metal) which results in a decrease of the width of the SCR. For a p-type semiconductor, this holds for negative applied voltages. The effect of different biasing conditions on the energy band positions of both n- and p-type doping, is illustrated in Figure 5.

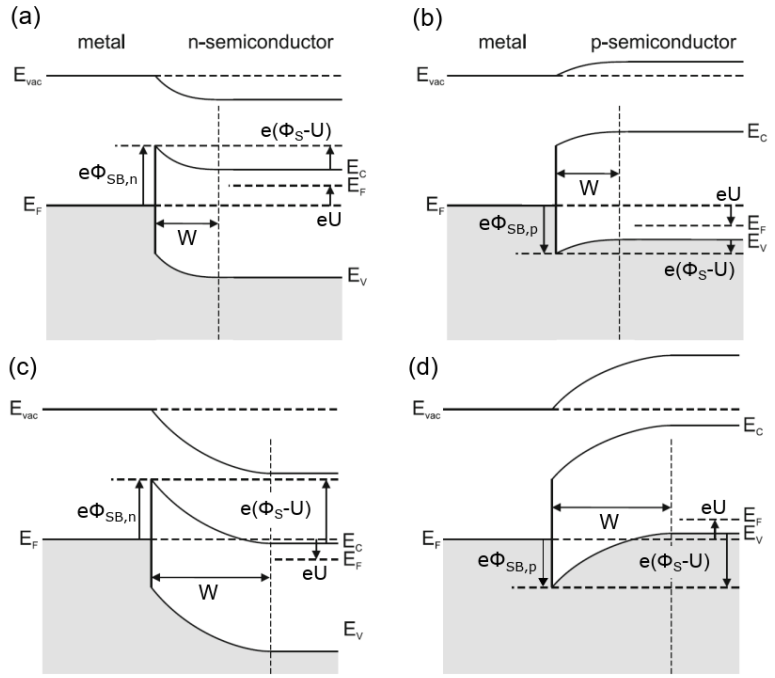

Figure 5: Semiconductor/metal junction for an n- and p-type semiconductor with (a) and (b) a forward bias applied (U > 0), and (c) and (d) for reverse bias (U < 0) [3].

For an n-type semiconductor, a forward bias of $U > 0$ leads to a decrease of $\Phi_{S,n}$ and W_n (Figure 5(a)). In contrast, a reverse bias ($U < 0$), leads to an increase of $\Phi_{S,n}$ and W_n (Figure 5(c)). Similar arguments hold for p-type material, but with an opposite polarity for forward and reverse bias conditions. Depending on the current-voltage characteristics, two different kinds of metal contacts on semiconductors can be distinguished: ohmic and rectifying contacts. Whether the current is directly proportional to the voltage or rectifying, depends on the width and height of the Schottky barrier [5]. As the current-voltage behavior strongly in influences the performance characteristics of a device, the right choice of contact material for the semiconductor of interest is an important prerequisite. An ohmic contact has a negligible junction resistance compared to the total resistance of the semiconductor device and, thus, does not significantly perturb the device performance [6]. Three mechanisms lead to low contact resistance: (i) a low barrier height for carrier transport, (ii) an accumulation layer without any barrier and (iii) high doping level, as this decreases the depletion width and, therefore, enhances the tunneling probability for charge carriers. For large band gap semiconductors, ohmic contact formation is generally difficult since the availability of material with a low enough work function to yield a low potential barrier is challenging [3].

2.3 The semiconductor/liquid electrolyte interface

In order to address the challenge of efficient solar light conversion into useful chemical energy, understanding the processes that occur at the semiconductor/electrolyte interface is of critical

importance. Since the 1950s, many studies have been focused on the investigation of this interface [7] [8] [9] [10] [11]. In contrast to semiconductors, current flow in solution occurs via the transport of ions rather than electrons. Charge transfer reactions taking place at the interface between electron (or hole) conductor and an ion conductor in solution are called electrochemical reactions. Thereby, electron transfer is inseparably linked to the oxidation or reduction of ions or molecules at the interface.

In a solution, ions are surrounded by a solvation shell of polar solvent molecules and other ions or molecules of the solution. This solvation shell is rearranged when electrons are transferred to or from the solvated ion, as it strongly depends on the charge of the ion. Solvated ions that can be oxidized and reduced by pure electron transfer are called redox couples. The tendency of a species to accept or release an electron when approaching an electrode or other ions is characterized by the chemical potential μ_i of the ion i [12]. When neglecting interactions between ions in an aqueous solution, μ_i can be approximated as:

$$\mu_i = \mu^0{}_i + RT \ln c_i$$

where $\mu^0{}_i$ is the standard chemical potential, c_i the ion concentration, R the ideal gas constant, and T the temperature. The chemical potential, combined with the electrostatic potential, Φ, of an ion i with charge z_i, results in the electrochemical potential $\tilde{\mu}_i$ which can be written as:

$$\tilde{\mu}_i = \mu_i + z_i F \Phi$$

with $F = eN_A$ being the Faraday constant, which is the product of elementary charge and Avogadro's number. In general, a redox reaction between an electron accepting and an electron donating species in equilibrium can be described by the following reaction equation:

$$Red \rightleftharpoons Ox + e^-$$

For this reaction to occur, the electrochemical potentials of the oxidizing and reducing species must be equal. The electrochemical potential of a transferred electron is given by [13]:

$$\tilde{\mu}_{e,redox} = \tilde{\mu}_{red} - \tilde{\mu}_{ox}$$

Combining the equations listed above, the resulting equation for the electrochemical potential of the redox couple $\tilde{\mu}_{e,redox}$, the so-called Nernst equation, is:

$$\tilde{\mu}_{e,redox} = \tilde{\mu}^0_{e,redox} + k_B T \ln \frac{c_{ox}}{c_{red}}$$

Here, c_{ox} and c_{red} are the concentrations of the oxidized and reduced species.

Generally, the Fermi level $E_{F,redox}$ of the redox system in a diluted solution is equal to the electrochemical potential $\tilde{\mu}_{e,redox}$. As Fermi levels are usually given in eV and refer to single electrons, $\tilde{\mu}_{e,redox}$ can be converted by [13]:

$$E_{F,redox} = \left(\frac{e}{F}\right) \cdot \tilde{\mu}_{e,redox}$$

While Fermi levels are commonly referred to the vacuum level in solid state physics, electrochemical potentials are usually given with respect to a reference electrode such as the standard hydrogen electrode (SHE). By definition of the SHE, the standard redox potential $\tilde{\mu}^0{}_{H^+/H2}$ of the H^+/H_2 redox couple on an inert platinum electrode under ambient pressure and room temperature is set to zero.

As $\tilde{\mu}^{0}_{H^+/H2}$ is located at approximately -4.5 eV with respect to the vacuum level, the following relation between the Fermi level of a redox couple in eV and its electrochemical potential versus SHE in V is valid:

$$E_{F,redox} = -4.5eV + \frac{e}{F}\tilde{\mu}_{e,redox}$$

The two different scales are compared in Figure 6 and the electrochemical potentials of various redox couples are given both versus vacuum level in eV and versus SHE in V.

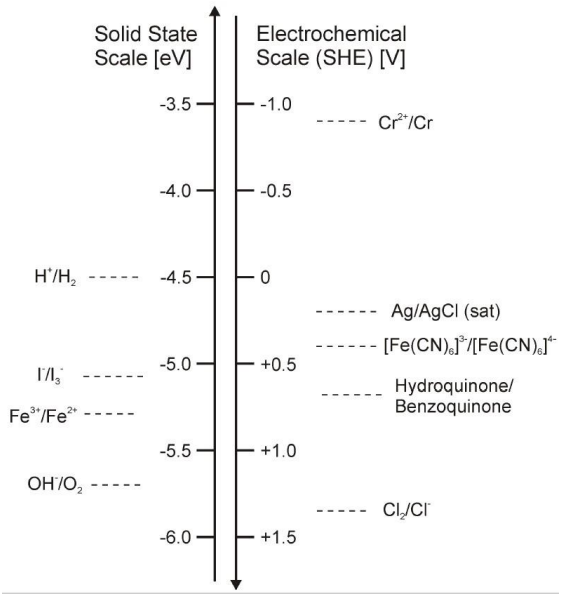

Figure 6: Electrochemical potentials of various redox systems given on the solid state scale versus the vacuum level in eV and on the electrochemical scale versus the standard hydrogen electrode (SHE) in V. Figure adapted from [14].

When a semiconductor is immersed in a redox electrolyte, charge carriers will flow from one phase to the other until the difference in the Fermi levels E_F of the semiconductor and $E_{F,redox}$ of the redox electrolyte are equal. For an ideal n-type semiconductor in the absence of surface states, electrons will transfer from the semiconductor into the solution. Much like for the case of metal-semiconductor contacts, the removal of electrons near the semiconductor surface results in a depletion layer containing positively charged donor ions which leads to a SCR with a certain width. The SCR corresponds to an upward band bending for an n-type semiconductor with a built-in voltage Φ_S. Figure 7(a) illustrates the energetic situation in the vicinity of an n-type semiconductor-electrolyte interface without and with contact. In contrast, for a p-type semiconductor, a downward band bending arises and the built-in voltage carries opposite sign (Figure 7 (b)) [15].

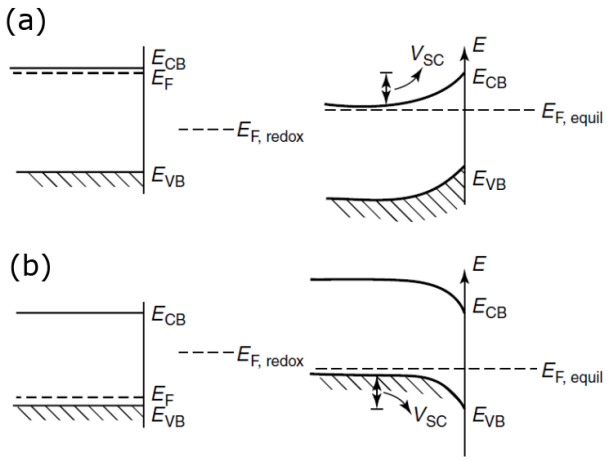

Figure 7: Energy levels of an (a) n- and (b) p-type semiconductor and a redox electrolyte in disequilibrium and in equilibrium when the two phases are in contact [24].

2.4 Photoelectrochemical water splitting

After introducing the fundamental band alignment of semiconductors in a liquid, this chapter now deals specifically with the photoelectrochemical mechanisms of solar water splitting.
Figure 8 shows a photoelectrochemical cell with a semiconductor photoanode and a metal counter electrode immersed into an electrolyte and electrically connected via an external wire.

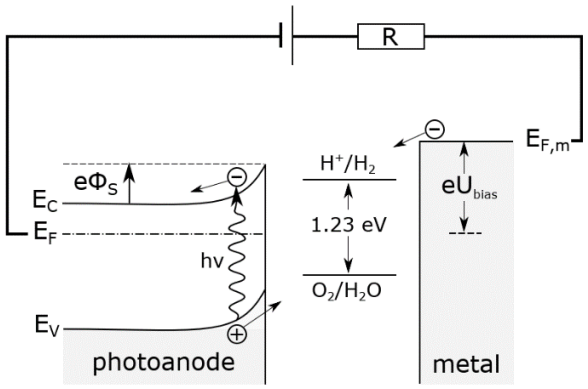

Figure 8: Photoelectrolysis by an n-type photoanode and a metal cathode under above-band gap illumination and an applied bias in diluted solution. Figure inspired by [16].

At their surfaces water is split into oxygen and hydrogen, respectively, when the required energy difference of at least 1.23 eV is provided. This value of 1.23 eV corresponds to the Gibbs free energy required to drive the energetically uphill water splitting reactions.

In darkness, the generation of H_2 or O_2 depends on the applied voltage U_{bias}. For the given example, in which hydrogen is evolved at a metal electrode poised at a sufficiently negative electrochemical potential, protons can be reduced to hydrogen when electrons move from the metal electrode into the electrolyte:

$$2H^+ + 2e^- \rightarrow H_2(g)$$

Likewise, the generation of oxygen occurs on the illuminated photoanode at sufficiently high positive potential. The corresponding anodic current originates from holes leaving the photoanode to cause the oxidation of hydroxide ions:

$$OH^- + 4h^+ \rightarrow 2H_2O + O_2(g)$$

As described above, the energy required to split one water molecule into hydrogen and oxygen is 1.23 eV. For solar-driven water splitting in the absence of an externally applied bias, both redox potentials for hydrogen and oxygen evolution must be covered by the band edges of the semiconductor electrode and are given by:

$$E_{H^+/H_2} = -(4.5 - 0.059 \cdot pH)eV$$

$$E_{OH^-/O_2} = -(4.5 + 1.23 - 0.059 \cdot pH)eV$$

When the energy for water splitting is not provided by an external voltage source but by photon energy, one speaks of photoelectrolysis. While in the dark majority charge carriers mainly promote electrochemical reactions, under illumination minority charge carriers dominate this process at the semiconductor surface [9] [17]. For successful water dissociation, the requirements for the semiconducting material are a minimum band gap of E_g =1.23 eV plus additional energy, the so-called overpotential, to drive the redox reaction in one direction. This overpotential accounts for catalytic barriers for the reactions, which are especially large for the oxidation reaction that evolves oxygen. In addition, series resistance losses in an non-ideal electrolytic cell must be overcome by the photovoltage generated within the semiconductor.

2.5 Internal efficiencies, kinetics and interfacial charge trapping

Even though semiconductors with suitable photoabsorption and band edge properties for solar water splitting have been identified, they still exhibit significantly lower experimental efficiencies than theoretically predicted. One of the most important limitations of photocatalysis for water splitting is that the process of simultaneous reduction and oxidation of water is a complex multistep reaction involving four electrons. A main research goal is to lower the kinetic barriers for the oxygen evolution reaction (OER).
When a semiconductor photoelectrode is illuminated with above band gap light, the conversion of the incident irradiance with power P_0 to a photocurrent density, J_{photo}, can be quantitatively analyzed by the following formula:

$$J_{photo} = P_0 \Phi_{abs} \Phi_{sep} \Phi_{inj}$$

where ϕ_{abs} is the photon absorption probability, ϕ_{sep} is the charge separation efficiency and ϕ_{inj} is the charge injection efficiency describing the yield of heterogeneous charge transfer across the semiconductor/electrolyte interface. The rate of photochemical reactions is strongly dependent on the competing processes of electron-hole pair photogeneration and their recombination. Surface recombination, which occurs at the defect sites present at semiconductor surfaces, can drastically lower the number of separated charge carriers available on the interface. In the absence of sacrificial reagents (i.e. redox couples in solution with very low kinetic barriers), the sluggish OER competes with

surface recombination and the accumulation of photogenerated holes and chemical rearrangements at the solid/liquid interface can form additional surface states within the band gap. This can lead to a reduction of the surface photovoltage and open up the possibility for other reaction pathways besides water dissociation (e.g. corrosion of the semiconductor).
When a sacrificial hole acceptor (e.g. Na_2SO_3) is added to the electrolyte, the charge carrier transport into the solution is rapid and the charge injection efficiency ϕ_{inj} is assumed to be near unity. This reduces the probability for surface recombination and is a powerful tool to investigate the internal semiconductor processes contributing to the interfacial charge transfer.

3 Bismuth vanadate: a high performance oxide photoanode for solar water splitting

3.1 Fundamental properties of $BiVO_4$

In this laboratory module, we will investigate a bismuth vanadate ($BiVO_4$) photoanode. $BiVO_4$ is a transition-metal oxide that has been actively investigated solar water splitting because it absorbs visible light and, thus, allows relatively efficient harvesting of the solar spectrum (see Figure 9).

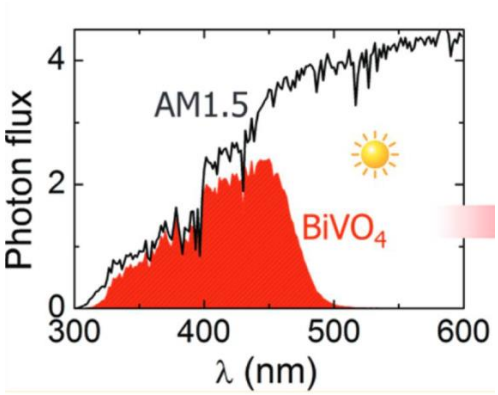

Figure 9: Spectrally resolved photon flux of AM1.5 sun light and, in red, the optical absorption capacity of $BiVO_4$ [18].

$BiVO_4$ has a moderate band gap of E_g = 2.5 eV, energetically favorable band edge positions for water splitting, and relatively long minority carrier diffusion lengths. It is one of the highest performance transition-metal oxide photoanodes and possesses a theoretical solar to hydrogen efficiency of up to 9.2% [1]. Despite these advantageous characteristics, the material also suffers from strong carrier localization [19], degradation via photocorrosion [20], and inadequately characterized defect properties. Current research focuses on improving understanding and establishing control of the electronic structure of $BiVO_4$, its photocarrier dynamics, defect physics, and chemical interactions. With the findings of these investigations on $BiVO_4$ as a model system, a general strategy can be derived to develop a sophisticated material design of transition-metal oxides for solar water splitting. In this laboratory module, we will conduct a systematic study of the photoelectrochemical properties of $BiVO_4$ and learn about the underlying *operando* mechanisms.

3.2 Synthesis of the $BiVO_4$ thin films used as photoelectrodes

The $BiVO_4$ thin films investigated in this course were fabricated by metal organic decomposition using spin-coating to deposit an approximately 50 nm thick film. A precursor solution containing metal-

organic compounds of the constituent elements, was mixed from two separately prepared solutions containing 0.2 M bismuth(III)nitrate pentahydrate and 0.03 M vanadium(IV)-oxy acetylacetonate, each dissolved in acetylacetone. The resulting precursor solution is spin-coated on cleaned fluorine-doped tin oxide (FTO) coated glass substrates and subsequently annealed in a muffle furnace at 500 °C for 10 min in air at ambient pressure. The sample annealing is required to decompose the metal organic precursors and form new chemical bonds. This process is known as pyrolysis and results in an inorganic thin film. With a final two hour long annealing step at 500 °C, the grain size and crystal quality of the polycrystalline grown $BiVO_4$ film can be improved. Figure 10 shows an atomic force micrograph of a polycrystalline $BiVO_4$ surface in which the typical nm-scale grain morphology of the polycrystalline film becomes clear.

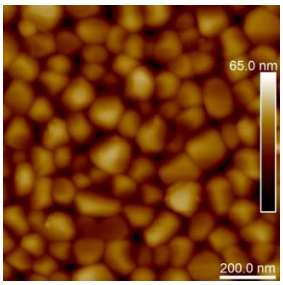

Figure 10: Atomic force microscopy image of a typical polycrystalline $BiVO_4$ surface showing the characteristic nm-size grains.

The FTO is a transparent conductor that provides ohmic electrical contact to the back of the $BiVO_4$, while also permitting light transmission. In particular, it has a sheet resistivity of approximately 10 Ω/cm^2. This high conductivity enables the fabrication of back-contacted $BiVO_4$ working electrodes for photoelectrochemical (PEC) measurements. Another advantage of these substrates is their transparency of approximately 80% in the visible range, allowing front- and backside illumination of the semiconducting $BiVO_4$ film.
After growth, the sample is cut into quadratic pieces with side dimensions of approximately 1 cm. On the edge of the sample, an approximately 2x3mm^2 wide $BiVO_4$ strip is treated with 0.2 M hydrochloric acid (HCl) until the semiconductor layer is removed and the conductive, transparent FTO substrate is exposed. This allows for electrical contact by an external lead.

4 Experimental setup

For the investigation and development of efficient and stable $BiVO_4$ photoelectrodes for solar water splitting, knowledge about the fundamental electrochemical behavior of the material is essential. For the systematic investigation of charge transfer across the $BiVO_4$/electrolyte interface, processes taking place during electrochemistry in the dark and under illumination with light with a sun-like spectrum, are analyzed.

4.1 Photoelectrochemical cell

In this laboratory module, a specially designed quartz glass beaker with an integrated quartz window (optical transmission from 200 to 2000 nm) is used that allows the illumination of the sample under normal incidence. The measurements are performed in a three-electrode configuration consisting of a silver/silver chloride (Ag/AgCl) reference electrode (RE), a spirally coiled inert Pt-wire counter electrode (CE), and an electrically contacted $BiVO_4$ sample as the working electrode (WE) (see Figure 11).

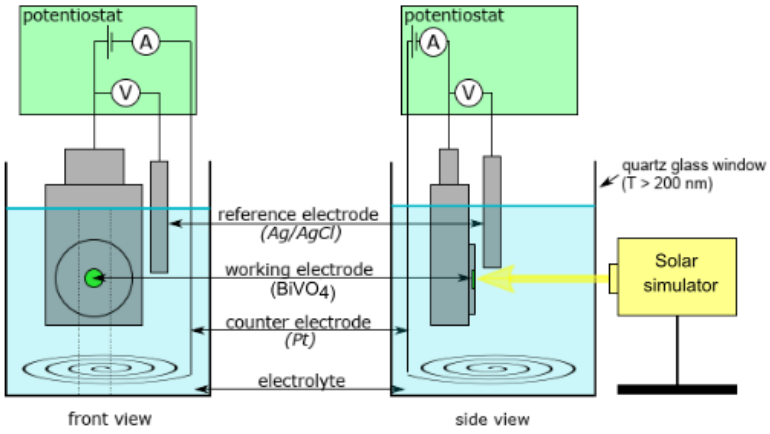

Figure 11: Sketch of the three-electrode setup consisting of a $BiVO_4$ working electrode, a Ag/AgCl reference and a Pt counter electrode immersed into an aqueous electrolyte and connected with a potentiostat. The dashed lines represent a UV light-transmitting quartz glass window which allows illumination with a solar simulator at normal incidence for photoexcitation.

The electrodes are immersed into an aqueous potassium phosphate (KPi) buffer solution at near neutral pH and are connected with a Gamry Reference 600+ potentiostat. A solar simulator equipped with an AM 1.5G filter is used to photoexcite the semiconductor electrode with light with a sun-like spectrum and its intensity is calibrated with a silicon reference cell to match the 1 sun intensity of 100 mW/cm^2. For measurements that require a quick sequence of dark and photoexcited states, an optical beam shutter is placed between the PEC cell and the solar simulator and is opened and closed by a separate controller.

The role of the reference electrode

The reason to use a third electrode, the reference electrode, in addition to the working and counter electrode is to be able to control the applied potential. It is crucial for the design and investigation of any electrochemical device to have precise knowledge of the electrode potential. When current flows through an electrochemical cell and chemical reactions take place, it can alter the chemical composition or electronic states of the electrode surfaces, thus changing their electrode potential. However, for a meaningful measurement, a constant reference is required to determine a potential difference between two electrodes since the absolute potential of one electrode can generally not be measured experimentally. To determine a well-defined value for the electrode potential one typically measures or applies a potential between the working and a reference electrode. Reference electrodes are made of ideally non-polarizable materials that practically remain unchanged when small currents are transferred and are chosen suitably depending on the specific conditions, such as the type of electrolyte or the currents that are flowing [21]. Common reference electrodes used in aqueous solutions are, among others, the Ag/AgCl electrode and the internationally accepted reversible hydrogen electrode (RHE). In this laboratory course we will measure potentials with respect to a Ag/AgCl reference electrode whose relative potential can be converted to be relative to the RHE by the following formula [12]:

$$E_{RHE} = E_{Ag/AgCl} + (pH \cdot 0.059\ \mathrm{V}) + 0.21V$$

Here, 0.21 V is the potential of the Ag/AgCl reference electrode potential with respect to that of the standard hydrogen electrode in 3 M potassium chloride (KCl). This equation shows that E_{RHE} is dependent on the pH of the electrolyte. In Figure 12 the typical design of a Ag/AgCl reference electrode is shown. A saturated 3 M KCl solution surrounds the Ag wire and the AgCl, therefore, it is important to prevent the electrode from drying out. A fine diaphragm separates the KCl solution from the supporting electrolyte and allows a voltage to be applied.

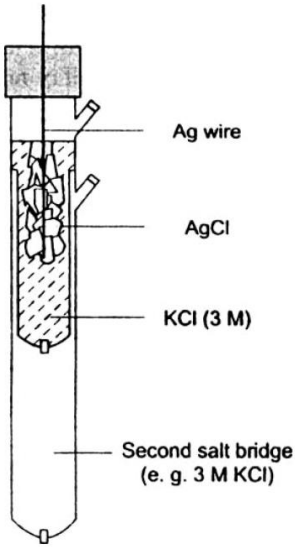

Figure 12: Structure of a silver/silver chloride reference electrode with a second 3 M KCl salt bridge.

In order to minimize the ohmic potential drop between reference and working electrode, the two electrodes should be positioned as close as possible and in a reproducible way [21].

4.2 Function of a potentiostat

A potentiostat is used in three-electrode electrochemical experiments to control the potential difference between working and reference electrode. It adjusts the potential at the working electrode to maintain a defined level with respect to the reference electrode by adjusting the current between the working and the counter electrode, while ensuring that no current flows across the reference electrode. Chemically, this corresponds to maintaining a flow of electrons required to trigger redox reaction processes at rates consistent with the desired potential [12]. The potentiostat measures the current while keeping control of the voltage. Figure 13 shows a simple schematic of the structure of a potentiostat [22].

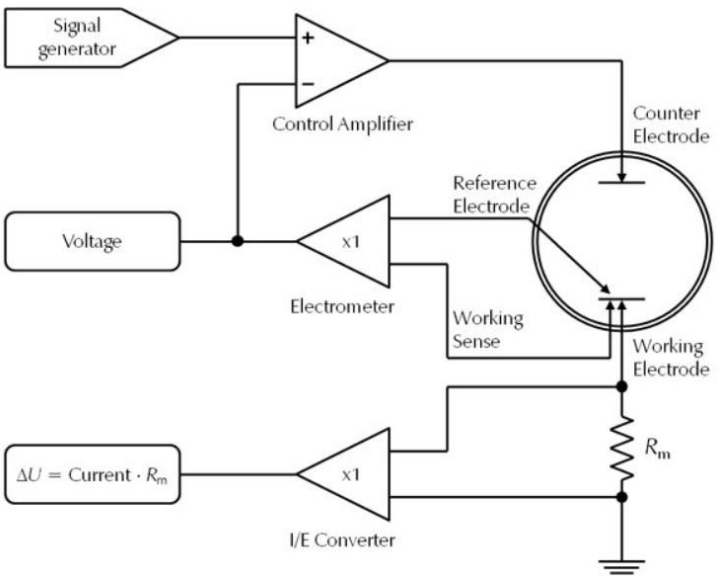

Figure 13: Schematic of a potentiostat connected to a three-electrode PEC cell [22].

A *Signal Generator* generates a specific signal form that is required for the desired electrochemical measurement (e.g. a ramp or a constant value) and a *Control Amplifier* amplifies that signal and adjusts its amplitude to match the desired input value. In this laboratory module we will use the potentiostat in the so-called *potentiostatic mode*, where a voltage is applied. When instead the applied signal is a current one speaks of the *galvanostatic mode*. With the *Electrometer*, the potential difference between working and reference electrode is measured, and the voltage value is sent to the *Control Amplifier*. A comparison between the target and the actual voltage value takes place in the *Control Amplifier*, and its output signal is adjusted to compensate for possible deviations. The *Current-to-Voltage Converter* (*I/E Converter*) measures the current between the counter and working electrode by converting the current to a voltage signal via a resistor R_m. The voltage drop ΔU across the resistor is proportional to the flowing current [22]. This functional design of the potentiostat allows to simultaneously control the voltage and measure the current through the electrochemical cell.

4.3 Electrochemical methods

Once the photoelectrochemical (PEC) cell is connected to the potentiostat, a systematic electrochemical analysis can be performed by applying different methods to monitor the charge transfer during electrochemical reactions. A common way for initial electrochemical studies of new electrode material systems is cyclic voltammetry (CV). This technique does not only allow the characterization of charge transfer across the semiconductor/electrolyte interface but also the monitoring of surface reactions such as corrosion and adsorption [12]. In a CV experiment, a linearly increasing voltage ramp with a constant scan rate v = dU/dt is applied between the working and the reference electrode, followed by a linearly decreasing voltage ramp, thereby forming a triangular shaped potential sweep, as illustrated in Figure 14(a).

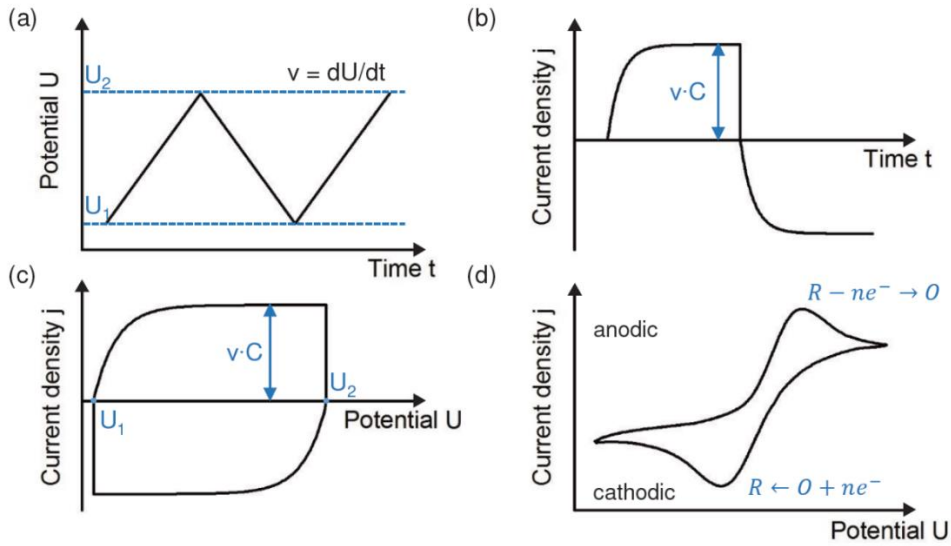

Figure 14: Measurement principle of cyclic voltammetry. (a) A DC bias is linearly increased and decreased with time between two switching potentials U_1 and U_2 with a constant scan rate v. (b) The resulting capacitive current density of the system is proportional to v and (c) typically plotted against the applied potential. The CV curve represents the current response of a system without Faradaic charge transfer across the electrode/electrolyte interface, which can be modeled by an equivalent RC circuit. (d) If charge transfer occurs during oxidation and reduction reactions, Faradaic current peaks can be observed in CV curves. Figure adopted from [23].

The resulting current density, *j*, between working and counter electrode is monitored simultaneously (see Figure 14(b)). An electrochemical cell can be modeled by an equivalent circuit model of a

resistance R_s, which represents ohmic resistances of the bulk electrode and the solution, and the electrolyte double layer capacitance, C_d, which originates from ions separated a short distance from the electrode by their solvation shell, thereby forming a capacitor-like double layer [12]. If no reactions take place and no Faradaic current flows, only a charging current density, j_c, can be observed, which is always present as a result of charging and discharging of C_d during a continuously changing potential [24]. j_c is then given by [12]:

$$j_c = \nu C_d \left[1 - exp\frac{-t}{R_s C_d}\right]$$

Thus, the charging current density is proportional to the scan rate v and increases until it saturates at a steady-state value vC_d when the voltage has reached its maximum value (see Figure 14(b)). This can later be used to experimentally estimate the electrolyte double layer capacitance, C_d [12]. For a triangular potential form, the steady-state current changes from vC_d to $-vC_d$. Typically, the current response of the system is plotted as current-voltage curves, so-called cyclic voltammograms. In Figure 14(c), the current response of a system is illustrated where no charge is transferred into the electrolyte and, thus, can be modeled by an equivalent circuit model consisting of a resistance and a capacitance in series. If charge is transferred across the electrode/electrolyte interface during reduction and oxidation reactions, Faradaic current peaks can be observed in CV curves, as depicted in Figure 14(d) [12]. For reversible processes, the peak current density j_p, measured from a baseline of charging current, is proportional to the square root of the scan rate $v^{1/2}$ (in $V^{1/2}$ $s^{1/2}$) according to [12]:

$$j_p = 0.44 \cdot \frac{(nF)^{\frac{3}{2}}}{(RT)^{\frac{1}{2}}} \cdot ACD^{\frac{1}{2}}\nu^{\frac{1}{2}}$$

where A is the electrode area (in cm^2), C the bulk concentration of reactants in the electrolyte (in mol/cm^3) and D the diffusion coefficient in (cm^2/s).

The modulated light measurements in this laboratory module will be performed with linear sweep voltammetry (LSV) which is a similar technique to CV, however, instead of sweeping the potential several times, only one single linear voltage sweep from lower to higher voltages with a constant scan rate is performed and the current is detected.

5 Course assignments

Before starting to work in the lab, please make yourself familiar with the safety instructions for this lab and the setup components and controls. You will get a lab safety introduction from your supervisor. Always make sure to wear suitable gloves when handling chemicals, the sample or optical components, and wear safety goggles when operating the solar simulator and handling chemicals. Ask your supervisor whenever there are uncertainties or questions of any kind. Additionally, please create a folder for all the files you will record during the course under: DATA(E:)\My Gamry Data\Fopra\YYYY-MM-DD_groupNumber\. After finishing the course, your supervisor will send you the recorded data for your written report via email.

5.1 Experimental tasks

During your course you will prepare your own $BiVO_4$ photoelectrode and perform PEC experiments to identify crucial charge transfer processes across the $BiVO_4$/electrolyte interface. In the following, a description of the experimental tasks is given.

A. Electrical connection of the $BiVO_4$ photoelectrode

In order to electrically connect the $BiVO_4$ sample with the potentiostat, a wire needs to be connected to the sample and all electrically active areas that will be immersed into the electrolyte except the $BiVO_4$ film need to be insulated with a chemically inert epoxy. Before starting to work with the sample or any chemicals, make sure to always wear nitrile gloves and not expose skin to any chemicals. Take one of the 1x1 cm^2 prepared $BiVO_4$ sample pieces, place it on a glass slide on a Kimwipe and identify the approximately 2x3 mm^2 area that was already etched away with 0.2 M diluted HCl. The area appears transparent in contrast to the yellowish color of the $BiVO_4$ thin film. By the HCl treatment, the $BiVO_4$ was etched away and the conductive FTO is exposed, which serves as a back contact.

Remove approximately 3-4 mm of insulation at one end and 5-6 mm insulation at the other end of the provided copper wire. Mix part A (epoxy) and part B (hardener) of the CW2400 silver epoxy on a weighing boat with the provided plastic stick according to the epoxy's description: Mix equal amounts (1:1) by weight or volume of part A and part B. Mix it thoroughly for 2 min. Apply this conductive epoxy within 8 min on the exposed FTO and the 3-4mm exposed copper wire to connect them. Make sure to use sufficient epoxy to achieve a stable, flat electrical connection with the FTO but avoid contaminating the $BiVO_4$ thin film with the silver epoxy. Carefully place the glass slide with the wire-connected $BiVO_4$ sample on a cold hotplate and stabilize the wire/$BiVO_4$ configuration with the clamp stand on the table beside the hotplate. Make sure that neither the plastic insulation of the wire nor the clamp touch the hotplate. Only after everything is secured and you have checked that nothing touches the hotplate, turn on the hotplate and heat it up to 75 °C. This will decrease the curing time of the epoxy from 4 h to 15 min. When the hotplate has reached 75 °C, set a timer for 10 min. After 10 min have passed, turn off the hotplate and unplug it. During the 10 min waiting time, rinse the quartz beaker and the second glass beaker thoroughly and carefully with deionized (DI) water to remove any possible contaminations. Place them carefully upside down on a Kimwipe. Leave the sample cooling down on the hotplate and proceed with the electrolyte preparation in the meantime.

B. Electrolyte preparation

For the electrochemical measurements, a 1 M phosphate buffer solution (KPi) at pH 6.8 is provided. It was prepared with 0.25 M monobasic K_2HPO_4 and 0.25 M dibasic KH_2PO_4. Before filling the KPi solution in the quartz glass beaker, make sure the quartz beaker was thoroughly rinsed with DI water. Then fill approximately 150 ml of the KPi buffer solution into the quartz glass beaker up to the mark. Determine the pH of the solution with the pH meter. To do so, uncover the pH electrode, rinse it with DI water and immerse it into the electrolyte solution. Wait until the pH value has equilibrated and write down the pH value. Since the pH is dependent on the environment temperature, always write down the environment temperature as well. After you have determined the pH value, take the pH electrode out of the electrolyte, rinse it thoroughly with DI water and put it back into the 3 M potassium chloride (KCl) filled plastic vial.

For some measurements, a sacrificial hole acceptor is required in order to increase the injection efficiency of charge carriers into the electrolyte to approximately $\eta_{inj} \approx 1$. For this, take a glass beaker, rinse it with DI water and fill it with 150 ml KPi buffer solution. Subsequently, add 1.89 g of sodium sulfite (Na_2SO_3) to the KPi buffer solution.

C. Finalize the $BiVO_4$ working electrode

Carefully check if the conductive epoxy is fully cured. If so, stabilize the $BiVO_4$ electrode with a glass tube and seal the connection to the $BiVO_4$ sample with the chemically inert, black Microset epoxy. With the Microset epoxy, insulate all electrically active areas of the conductive epoxy but keep the $BiVO_4$ surface free of epoxy so that it can be exposed to the electrolyte. The Microset epoxy has a very short working time of only 30s, so be quick with the sealing. If cured, the epoxy has a silicone like consistency and can be easily removed with a fingernail.

D. Connect electrodes to the potentiostat

Turn on the Gamry potentiostat, but do not yet connect any electrodes to it.

Now that the working electrode and the electrolyte are prepared, the three electrodes can be immersed into the solution, suitably positioned, and fixed with clamps. Place the quartz beaker and the electrodes in the black box to avoid scattered ambient light. Make sure to handle the Ag/AgCl reference electrode and especially the sensitive grid at its end with care. The Ag/AgCl reference electrodes are stored in a 3 M KCl solution and should never dry out because that would break them. Before using the reference electrode and to avoid contaminations, rinse it thoroughly with DI water over a glass beaker. Then immerse it into the electrolyte and fix it with a clamp approximately 1 cm away from the working electrode without blocking the light beam from the solar simulator. Before immersing the working and counter electrode into the electrolyte, rinse both thoroughly with DI water over a big glass beaker to remove any possible contaminations prior to the measurements.

To avoid overshooting potentials in the Gamry potentiostat, it is crucial to connect the electrodes in a certain order and with the correct Gamry cable. Please see the color-coded description on the Faraday cage for the right order to connect the electrodes to the Gamry (see Figure 15). The order is reversed when unplugging the electrodes.

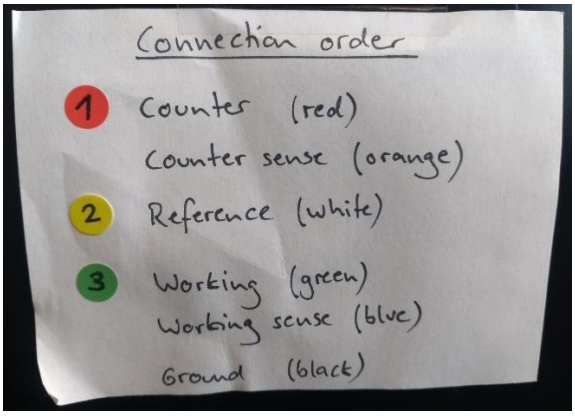

Figure 15: Connection sequence to connect the counter (red), reference (white) and working (green) electrode with the potentiostat.

Double check the position of the electrodes. Is the WE perpendicular to the incident light beam and is it fully illuminated by the solar simulator beam? Is the RE approximately 1 cm away from the WE without blocking the light? Are the three electrodes not touching each other?

E. Operating the Gamry Framework software

Open the *Gamry Framework* software by clicking on the icon on the desktop. Before starting a measurement please change the folder path to your groups' folder under > Options > Configure Paths > Data (DTA) "Browse" (see Figure 16).

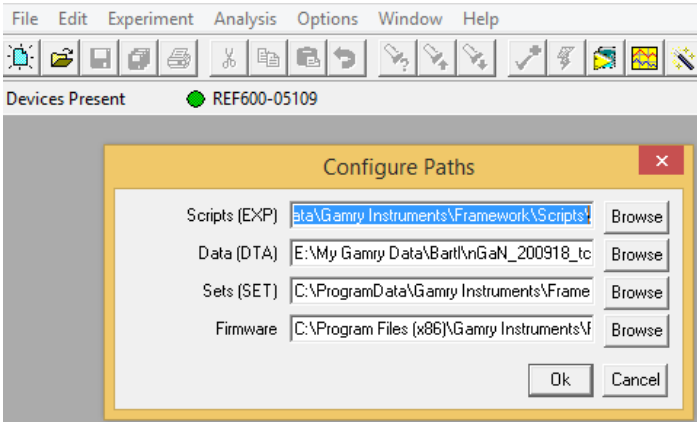

Figure 16: Change the file location to your group folder under > Options > Configure Paths > Data (DTA) "Browse".

Select the desired experiment in the list under > Experiment (see Figure 17).

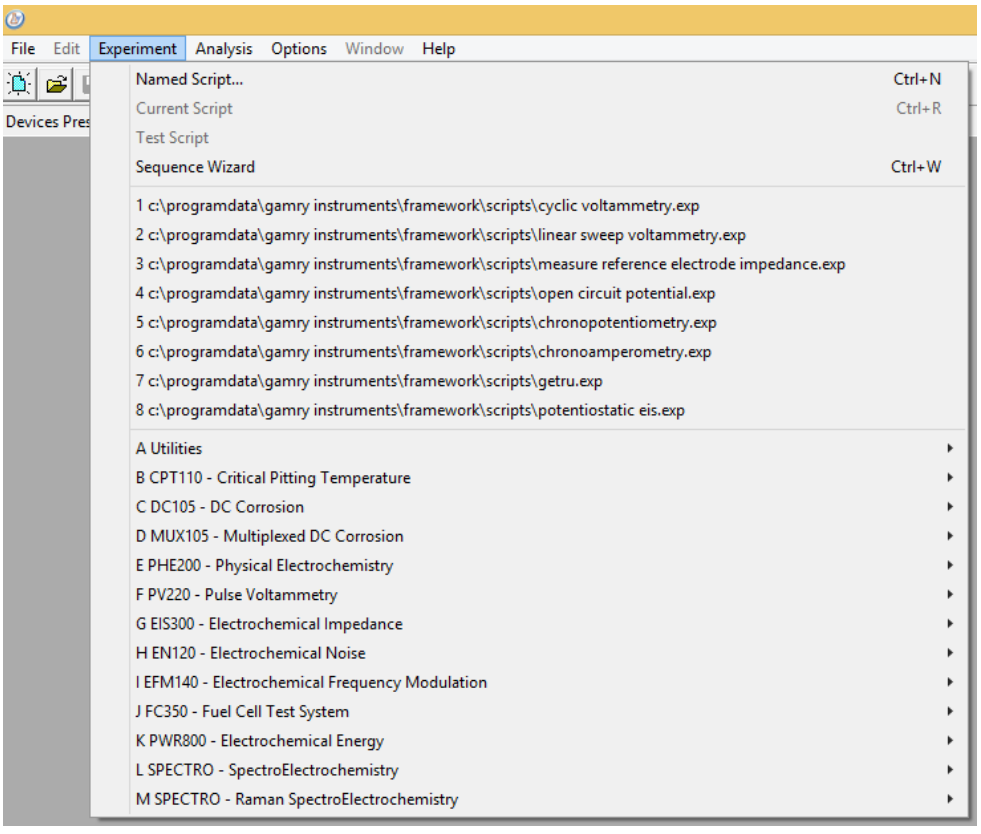

Figure 17: Select the desired experiment under > Experiment (e.g. cyclic voltammetry.exp).

In the parameter overview for the CV and the LSV experiment, set the respective measurement parameters accordingly as shown in Figure 18. Make sure to give a meaningful filename with the extension ".DTA" for each measurement (e.g. "fs-illum-CV_KPi_with_Na2SO3.DTA" with "fs-illum" for frontside illumination).

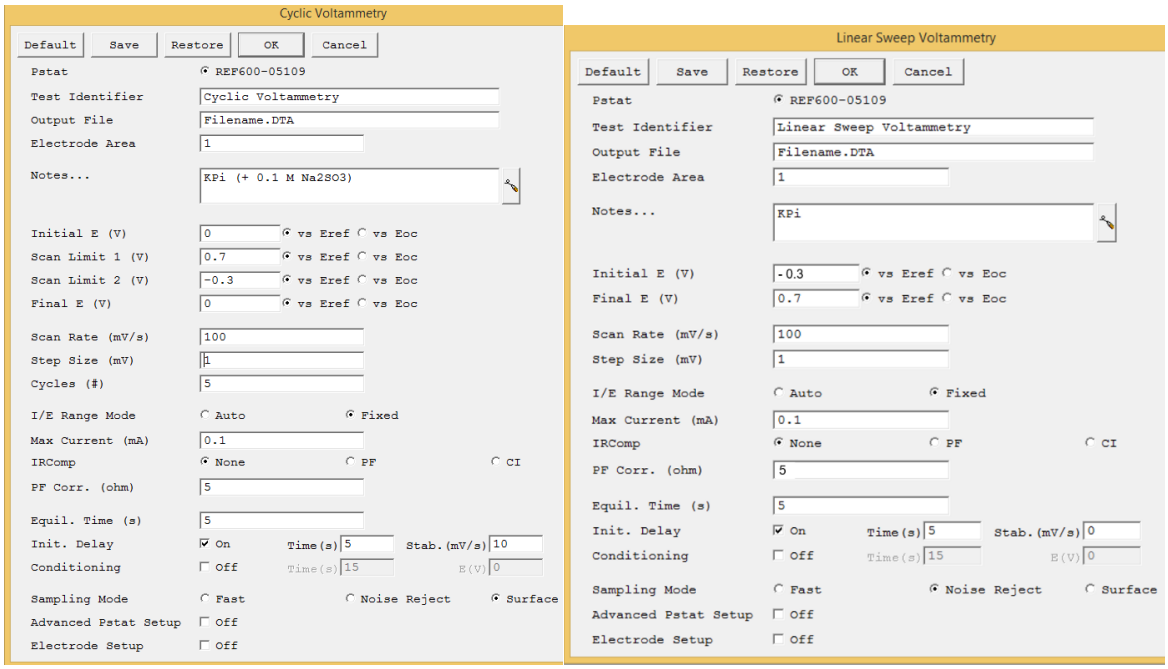

Figure 18 : Measurement parameters for cyclic voltammetry and linear sweep voltammetry.

Clicking “OK” will start the measurement immediately. After a measurement is completed, you can close the measurement window by pressing “F2”. This will automatically save the measurement under the previously assigned output filename in your selected group folder.

F. Start the PEC experiments

After everything is set up, you are ready to start measuring according to the following measurement sequence for a systematic PEC characterization of the prepared $BiVO_4$ photoanode.

1) Measure CV in the dark in the pure KPi electrolyte (without the sacrificial hole acceptor Na_2SO_3). Adjust the scan rate, step size, maximum current range and the electrochemical potential window according to Figure 18. Make sure to change the filename for each measurement.
2) Change the electrolyte to the KPi solution with Na_2SO_3 added, check the positions of the three electrodes and repeat the CV scan of step 1) in the dark.
3) Open the shutter of the solar simulator and record a CV for both frontside and backside illumination of the $BiVO_4$ working electrode. For backside illumination, turn the $BiVO_4$ working electrode by 180° and make sure that it is again aligned with the light at the normal angle of incidence and that the whole WE area is illuminated.
4) Change the electrolyte once more back to the pure KPi buffer solution (without Na_2SO_3). Before filling in the pure KPi buffer solution, thoroughly rinse the quartz beaker with DI water to remove any traces of Na_2SO_3. Then repeat the illuminated frontside and backside CV measurements of step 3).
5) To record LSV scans under chopped illumination, make sure that the frontside of the $BiVO_4$ is facing the solar simulator. Adjust the LSV parameters according to Figure 18 and the frequency of the beam shutter to the value given by your supervisor.

G. Finishing the experiment

After you made sure that you successfully finished all experiments, made notes about the relevant measurement parameters and that all data was stored in your group folder, notify your supervisor that you finished the experiments. We will have a concluding conversation about the course.
After we finished the course together, turn off the solar simulator and the controller for the beam shutter. Then disconnect the electrodes from the potentiostat in the revers order as they were connected (see Figure 15). Shut off the potentiostat, take the electrodes out of the solution and rinse them with DI water over a glass beaker. Carefully place the Ag/AgCl electrode back in the 3 M KCl storage bottle and seal it with parafilm. Rinse the Pt wire with DI water, dry it under a N_2 stream and carefully wrap it in a Kimwipe. After rinsing, place the $BiVO_4$ working electrode in the provided storage box. Dispose of the electrolytes in the container provided by your supervisor, and rinse the beakers thoroughly with DI water. Leave the glassware upside down on a Kimwipe on the table to dry.

5.2 Written lab report

Please write a conclusive report about the experiments you have performed in this course, including your results in the form of meaningful plots with all axes and legends clearly labeled. Analyze and discuss your observations. Please work through the following tasks:

- Calculate the current densities by estimating the electrochemically active area of the $BiVO_4$ working electrode. For all plots, give the electrochemical potential with respect to the reversible hydrogen electrode (RHE). Make sure to indicate which measurements were performed with and without sacrificial reagent, with front- or backside illumination, and under darkness or light.
- Plot the current densities obtained in the dark and under continuous front- and backside illumination versus the applied electrochemical potential (vs. RHE). Provide one plot for the measurements without sacrificial reagent and one with sacrificial reagent. Show only the second cycle of each CV. Describe the physical reason for differences between the light and dark curves. Considering the power incident on the sample under 1 sun illumination conditions, discuss whether the $BiVO_4$ electrode functions efficiently.
- What do you notice when comparing the current densities obtained under frontside and under backside illumination? Provide an explanation for any observed differences by considering minority and majority carrier transport within the material.
- What does the onset potential of the current density tell you? How is the onset potential affected by the presence or absence of sacrificial reagent? Discuss why this difference might be observed.
- Determine and plot the charge separation efficiency as a function of the applied electrochemical potential for the case of frontside and for the case of backside illumination.
- Plot the current densities under chopped illumination versus applied electrochemical potential (vs. RHE). Using these data, calculate the trapped charge density, i) near the onset potential, and ii) at the reversible potential for oxygen evolution. Describe and explain any differences to the photocurrent transients that you observed with and without sacrificial hole acceptor. For developing efficient photoelectrodes, should one try to minimize or maximize these photocurrent transients, why?

5.3 Colloquium: questions to answer

a. The 1 M KPi buffer solution that is provided for the PEC measurements is prepared from 0.25 M monobasic K_2HPO_4 and 0.25 M dibasic KH_2PO_4. Calculate how many grams of each chemical were added to 500ml DI water to obtain the final buffer solution.
b. During the laboratory, 1.89 g of the sacrificial hole acceptor Na_2SO_3 were added to 150 ml of the 1 M KPi buffer solution. How many moles of the sacrificial hole acceptor are now in the solution?

5 References

[1] D. MacKay, Sustainable Energy-without the hot air, UIT cambridge, 2008.

[2] Z. Zhang and J. T. Yates, "Band Bending in Semiconductors: Chemical and Physical Consequences at Surfaces and Interfaces," vol. 112, pp. 5520-5551, 2012.

[3] M. Grundmann, Physics of semiconductors, vol. 11, Berlin: Springer, 2010.

[4] W. Schottky, "Halbleitertheorie der Sperrschicht," vol. 26, pp. 843-843, 1938.

[5] E. H. Rhoderick, "Metal-semiconductor contacts," vol. 129, p. 1, 1982.

[6] S. M. Sze and K. K. Ng, *Physics of Semiconductor Devices,* 2006.

[7] W. Brattain and C. Garrett, "Electrical properties of the interface between a germanium single crystal and an electrolyte," *Physical Review,* vol. 94, no. 750, 1954.

[8] H. Gerischer, "Über den Ablauf von Redoxreaktionen an Metallen und an Halbleitern," vol. 27, pp. 48-79, 1961.

[9] H. Gerischer, "Charge transfer processes at semiconductor-electrolyte interfaces in connection with problems of catalysis," vol. 18, pp. 97-122, 1969.

[10] M. Gleria, "Charge transfer processes at large band gap semiconductor electrodes: reactions at SiC-electrodes," vol. 65, pp. 163-175, 1975.

[11] R. Beranek, "(Photo)electrochemical Methods for the Determination of the Band Edge Positions of TiO2-Based Nanomaterials," vol. 2011, pp. 1-20, 2011.

[12] A. J. Bard, L. R. Faulkner, J. Leddy and C. G. Zoski, Electrochemical methods: fundamentals and applications, New York: John Wiley & Sons, 2001.

[13] R. Memming, *Semiconductor Electrochemistry,* 2000.

[14] S. Schäfer, "Electronic control of catalytic activity," PhD thesis, WSI, TUM, Garching, 2013.

[15] K. Rajeshwar, *Fundamentals of Semiconductor Electrochemistry and Photoelectrochemistry,* 2002.

[16] T. Bak, J. Nowotny, M. Rekas and C. C. Sorrell, "Photo-electrochemical hydrogen generation from water using solar energy. Materials-related aspects," vol. 27, pp. 991-1022, 2002.

[17] H. Gerischer, "The role of semiconductor structure and surface properties in photoelectrochemical processes," vol. 150, pp. 553-569, 1983.

[18] F. F. Abdi and R. van de Krol, "Nature and Light Dependence of Bulk Recombination in Co-Pi-Catalyzed BiVO4 Photoanodes," vol. 116, pp. 9398-9404, 2012.

[19] A. J. E. Rettie, W. D. Chemelewski, D. Emin and C. B. Mullins, "Unravelling Small-Polaron Transport in Metal Oxide Photoelectrodes," vol. 7, pp. 471-479, 2016.

[20] F. M. Toma, J. K. Cooper, V. Kunzelmann, M. T. McDowell, J. Yu, D. M. Larson, N. J. Borys, C. Abelyan, J. W. Beeman, K. M. Yu, J. Yang, L. Chen, M. R. Shaner, J. Spurgeon, F. A. Houle, K. A. Persson and I. D. Sharp, "Mechanistic insights into chemical and photochemical transformations of bismuth vanadate photoanodes," vol. 7, 2016.

[21] A. J. e. a. Bard, Electrochemical dictionary, Leipzig: Springer-Verlag Berlin Heidelberg, 2008.

[22] G. Instruments, "Applications Notes: Understanding the Specifications of your Potentiostat," Gamry Instruments, 2020. [Online]. Available: https://www.gamry.com/application-notes/instrumentation/understanding-specs-of-potentiostat/. [Accessed 15 11 2020].

[23] M. Sachsenhauser, "Functional silicon carbide electrodes for applications in bioelectronics and biosensing," PhD thesis, WSI, TUM, Garching, 2017.

[24] S. R. Morrison, *Electrochemistry at Semiconductor and Oxidized Metal Electrodes,* 1980.

[25] Y. Pihosh, I. Turkevych, K. Mawatari, J. Uemura, Y. Kazoe, S. Kosar, K. Makita, T. Sugaya, T. Matsui, D. Fujita, M. Tosa, M. Kondo and T. Kitamori, "Photocatalytic generation of hydrogen by core-shell WO3/BiVO4 nanorods with ultimate water splitting efficiency," vol. 5, 2015.

[26] Y. Park, K. J. McDonald and K.-S. Choi, "Progress in bismuth vanadate photoanodes for use in solar water oxidation," vol. 42, pp. 2321-2337.

[27] Y. Park, K. J. McDonald and K.-S. Choi, "ChemInform Abstract: Progress in Bismuth Vanadate Photoanodes for Use in Solar Water Oxidation," vol. 44, pp. no-no, 2013.